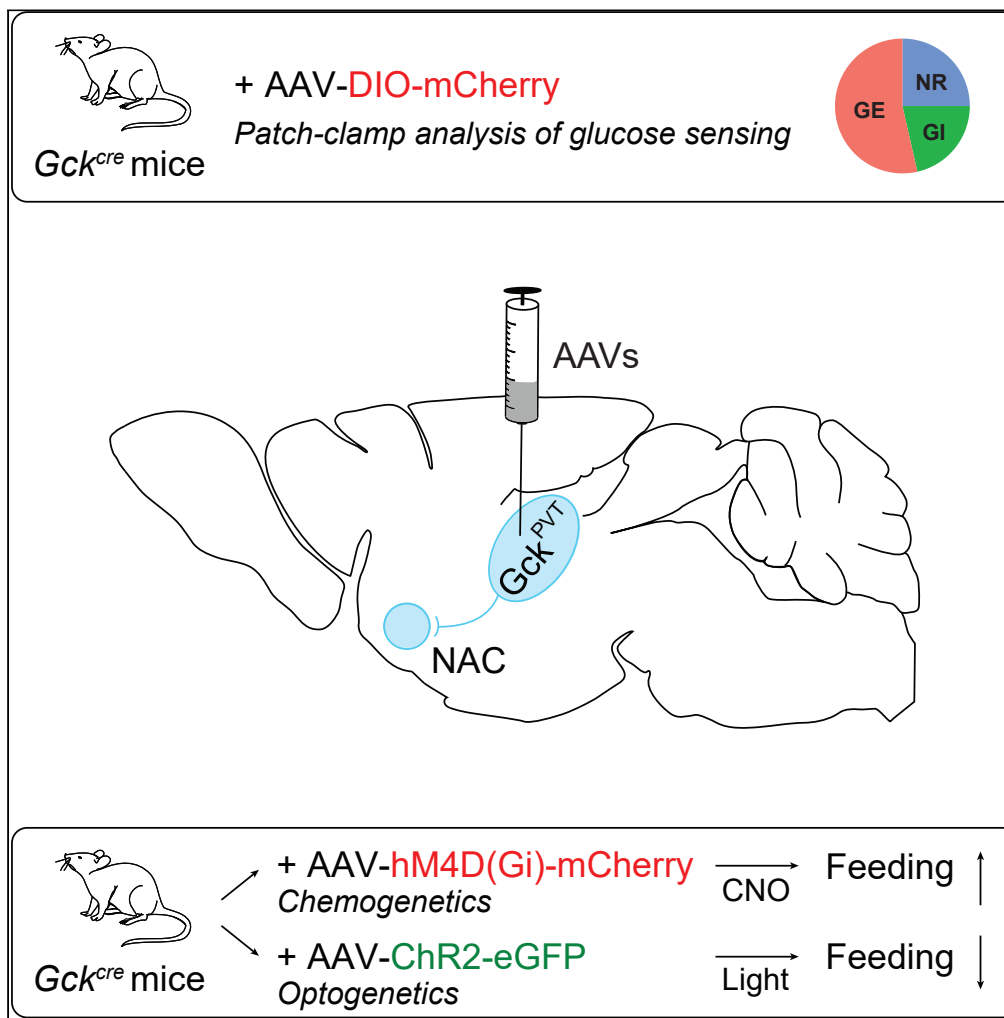


Article

Glucokinase neurons of the paraventricular nucleus of the thalamus sense glucose and decrease food consumption



Sébastien Kessler, Gwenaël Labouèbe, Sophie Croizier, Sevasti Gaspari, David Tarussio, Bernard Thorens

bernard.thorens@unil.ch

Highlights

Glucokinase (Gck) is expressed in neurons of the paraventricular thalamus (PVT)

Most Gck-expressing PVT neurons are glucose-excited neurons

Chemogenetic inhibition of the Gck^{PVT} neurons increases food intake

Optogenetic activation of accumbens-projecting Gck^{PVT} neurons decreases sucrose seeking

Kessler et al., iScience 24, 103122
October 22, 2021 © 2021 The Author(s).
<https://doi.org/10.1016/j.isci.2021.103122>

Article

Glucokinase neurons of the paraventricular nucleus of the thalamus sense glucose and decrease food consumption

Sébastien Kessler,^{1,2} Gwenaël Labouèbe,^{1,2} Sophie Croizier,^{1,2} Sevasti Gaspari,¹ David Tarussio,¹ and Bernard Thorens^{1,3,*}

SUMMARY

The paraventricular nucleus of the thalamus (PVT) controls goal-oriented behavior through its connections to the nucleus accumbens (NAc). We previously characterized $Glut2^{aPVT}$ neurons that are activated by hypoglycemia, and which increase sucrose seeking behavior through their glutamatergic projections to the NAc. Here, we identified glucokinase (*Gck*)-expressing neurons of the PVT (Gck^{aPVT}) and generated a mouse line expressing the Cre recombinase from the glucokinase locus ($Gck^{Cre/+}$ mice). *Ex vivo* calcium imaging and whole-cell patch clamp recordings revealed that Gck^{aPVT} neurons that project to the NAc were mostly activated by hyperglycemia. Their chemogenetic inhibition or optogenetic stimulation, respectively, enhanced food intake or decreased sucrose-seeking behavior. Collectively, our results describe a neuronal population of *Gck*-expressing neurons in the PVT, which has opposite glucose sensing properties and control over feeding behavior than the previously characterized $Glut2^{aPVT}$ neurons. This study allows a better understanding of the complex regulation of feeding behavior by the PVT.

INTRODUCTION

Changes in blood glucose concentrations induce hormonal and behavioral changes to restore normoglycemia and to control feeding behavior. Hypoglycemia triggers not only the secretion of counterregulatory hormones such as glucagon, epinephrine, norepinephrine, corticosterone, and growth hormone to induce endogenous glucose production, but also stimulates feeding and the absorption of sugar-containing food to replenish the body glucose stores (Marty et al., 2007; Verberne et al., 2014). In contrast, hyperglycemia leads to the secretion of insulin to augment glucose uptake by liver, fat, and muscles, and to the suppression of food intake (Brüning et al., 2000; Saltiel and Kahn, 2001). The central nervous system plays an important role in the control of these physiological responses (Bentsen et al., 2019; Steinbusch et al., 2015), in particular through the involvement of glucose responsive neurons. These are either excited by a rise in glucose concentration (glucose excited or GE neurons) or by a fall in glycemia (glucose inhibited or GI neurons) (Hirschberg et al., 2020). Their role is to modulate the activity of the autonomic nervous system or of the hypothalamus-pituitary-adrenal axis to control glucose homeostasis, or the reward system to control feeding behavior.

Activation of GE neurons has been suggested to depend on a signaling pathway that resembles that of the pancreatic beta-cells. This requires glucose metabolism, initiated by the uptake of glucose by the glucose transporter *Glut2* and glucose phosphorylation by glucokinase. The resulting increase in ATP/ADP ratio closes a K_{ATP} channel, leading to plasma membrane depolarization and, in beta-cells, to insulin secretion or, in neurons, to increased firing activity (Ashcroft and Rorsman, 2012). Activation of GI neurons by hypoglycemia requires the activation of AMP-dependent protein kinase (Quenneville et al., 2020), closure of a chloride channel (Hirschberg et al., 2020), or inhibition of the Na^+/K^+ ATPase as a result of a fall in intracellular ATP levels (Kurita et al., 2015; Silver and Erecinska, 1998). However, the mechanisms of gluco-detection by GE and GI neurons are not fully characterized (Thorens, 2012). For instance, recent observations using genetic approaches have shown that, in contrast to previous conclusions (Kang et al., 2006), the glucose responsiveness of GE or GI neurons of the ventromedial nucleus of the hypothalamus (VMN) does not require *Gck* expression (Steinbusch et al., 2016). On the other hand *Glut2* was found to be a

¹Center for Integrative Genomics, University of Lausanne, Genopode Building, 1015 Lausanne, Switzerland

²These authors contributed equally

³Lead contact

*Correspondence:

bernard.thorens@unil.ch

<https://doi.org/10.1016/j.isci.2021.103122>



marker of GI neurons of the nucleus of the tractus solitarius (Lamy et al., 2014) and to be required for the regulation by glucose of the activity of GI neurons of the paraventricular nucleus of the thalamus (PVT) (Labouèbe et al., 2016). The mechanisms of neuronal gluco-detection are, thus, more diverse than those of the pancreatic beta-cells (Thorens, 2012), and Glut2 and Gck may play different roles in glucose signaling and even operate in separate cells.

The mesolimbic dopaminergic system plays a key role in reinforcing natural rewarding behaviors such as food seeking, and attributing incentive salience to external or internal cues (Berridge and Robinson, 1998; Novelle and Diéguez, 2018). It consists in its fundamental part of dopaminergic neurons of the ventral tegmental area (VTA) that send projections to the nucleus accumbens (NAc) and to the prefrontal cortex. Other neuronal pathways interact with the reward system to regulate the consumption of food, in particular those with high hedonic value, which contain high proportion of glucose and/or fat. One such input to the NAc is the PVT (Millan et al., 2017), a site that integrates enteroceptive information on body energy status, and links this information to the control of motivated behavior. Indeed, results from several studies showed that stimulating the PVT → NAc projections induced food aversion and rejection (Do-Monte et al., 2017; Hua et al., 2018; Lafferty et al., 2020; Zhu et al., 2016). In contrast, we recently described a pathway from the PVT to the NAc that stimulates sucrose-seeking behavior (Labouèbe et al., 2016). This study showed that Glut2^{aPVT} neurons, which constitute a homogenous population of GI neurons, stimulate food-seeking behavior when depolarized by hypoglycemic conditions. Those contradicting findings lead us to suppose that the PVT → NAc pathway consists in a heterogenous population of neurons able to trigger opposite effects on food-seeking behavior.

Here, we characterized *Gck* expression in the PVT using *in situ* hybridization techniques, and mice that express the Cre recombinase from the *Gck* locus. We found that *Gck*^{aPVT} neurons are mostly GE neurons and their chemogenetic inhibition increases food intake, while their optogenetic activation reduces food-seeking. Our results demonstrate the presence of a population of glucose responsive neurons in the PVT characterized by the expression of *Gck*, and which exhibit opposite glucose responsiveness and control over motivated feeding behavior as compared to the previously described Glut2^{aPVT} neurons (Labouèbe et al., 2016).

RESULTS

Gck^{aPVT} neurons project to the NAc shell

We first assessed the distribution of *Gck* mRNA in the anterior PVT (aPVT) by chromogenic *in situ* hybridization. *Gck*-expressing cells were present at highest density in the aPVT, and in sparse neurons of the adjacent paratenial thalamus (PT) (Figure 1).

To selectively investigate the properties and physiological functions of *Gck*-expressing cells we generated a transgenic mouse line by introducing the codon-improved Cre recombinase (Shimshek et al., 2002) before the stop codon of *Gck* present in exon 10, separated from the *Gck* sequence by a T2A ribosomal skipping sequence (de Felipe et al., 2003) (Figure 2A). To assess the distribution of *Gck*-expressing neurons, we injected an adeno-associated virus harboring a *hSyn-DIO-eGFP* construct in the aPVT of *Gck*^{cre/+} mice (Figure 2B). A strong eGFP signal was observed in the aPVT (Figure 2C), which showed similar distribution to that of *Gck* mRNA identified by *in situ* hybridization (Figure 2D). We also confirmed that all neurons that express the Cre recombinase (revealed by expression of the mCherry after injection of an AAV8-*hSyn-DIO-mCherry*) also expressed the *Gck* mRNA (Figure 2E).

Glucose responsiveness of *Gck*^{aPVT} neurons measured by Ca²⁺ transient analysis

As a first step to characterize the properties of the *Gck*^{aPVT} neurons we examined their glucose responsiveness using *ex-vivo* calcium imaging in acute brain slices. *Gck*^{cre/+} mice were injected in the aPVT with an AAV9 carrying a *syn-FLEX-jGCaMP7s-WPRE* construct (Dana et al., 2019) (Figure 3A). Four to eleven weeks after surgery, we prepared brain coronal sections (250 μm, −0.22 to −1.46 mm from Bregma), and measured the calcium response of *Gck*^{aPVT} neurons to a switch in the extracellular glucose concentration from 2.5 to 0.1 mM (15 min each; Figure 3B). We found that a majority (65%) of these neurons were inhibited by a decrease in the extracellular glucose concentration (GE neurons; Poisson GLMM-PQL: $t = 6.9$, adj. $p < 0.001$ and $t = 5.6$, adj. $p < 0.001$), while 27% were activated (GI neurons; Poisson GLMM-PQL: $t = -3.8$, adj. $p < 0.01$ and $t = -3.7$, adj. $p < 0.01$), and 8% did not exhibit a change of their calcium transient frequency (NR neurons) (Figures 3C and 3D). We then repeated this experiment while simultaneously

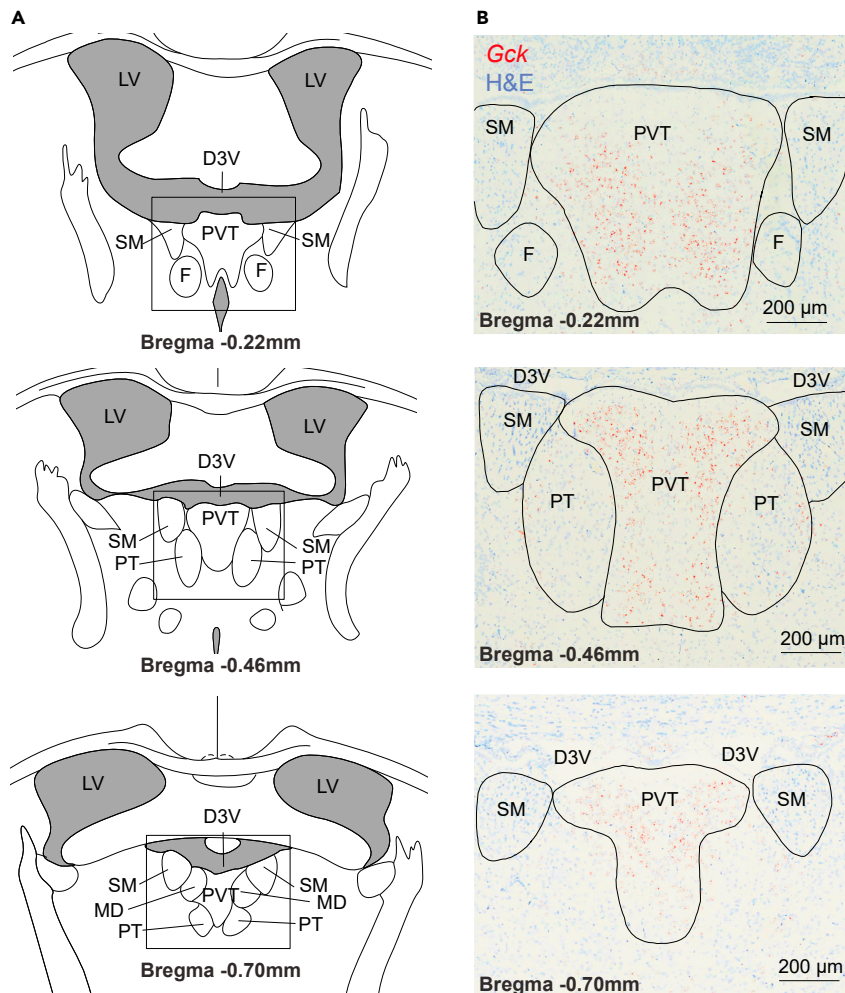


Figure 1. Distribution of the *Gck* mRNA expression in the anterior PVT of the mouse

(A) Schemes of coronal sections of the mouse brain at three different Bregma. (B) Detection of the *Gck* mRNA (red) by *in situ* hybridization at the corresponding Bregma and hematoxylin/eosin staining (H&E; purple). D3V: dorsal 3rd ventricle, LV: lateral ventricle, F: fornix; MD: medio dorsal thalamic nucleus; PVT: paraventricular thalamic nucleus, PT: paratenial thalamic nucleus, SM: stria medullaris.

blocking the synaptic transmission with a mixture of strychnine (glycine-gated chloride channels antagonist), DNQX (AMPA and kainate receptors antagonist), DL-AP5 (NMDA receptors antagonist) and picrotoxin (GABA_A receptors antagonist) (Figures 3E and 3F). GE, GI and NR neurons were still observed with non-significant change in the proportion of both GE (Binomial GLM with logit link, $\chi^2_{1,85} = 1.3$, $p = 0.26$) and GI neurons ($\chi^2_{1,85} = 0.7$, $p = 0.4$) in the presence of the inhibitors, indicating that their glucose sensing property was cell autonomous.

Glucose responsiveness of *Gck*^{aPVT} neurons projecting to the NAc

To investigate the glucose sensing properties of those *Gck*^{aPVT} neurons that project to the NAc we injected an AAV8-*hSyn-DIO-mCherry* in the aPVT of *Gck*^{cre/+} mice, and the retrograde tracer cholera toxin B subunit-Alexa Fluor 488 conjugate (CTxB-AF 488) bilaterally into the NAc (Figure 4A). We observed numerous mCherry-positive fibers in both the shell and the core of the NAc (Figure 4B). In the aPVT, we found a prominent co-labeling of Alexa Fluor 488 and mCherry (Figure 4C).

These double-labeled aPVT neurons were then investigated by whole-cell current-clamp recordings in 250 μm acute coronal brain slices (Bregma -0.22 mm to -1.06 mm). After a 7–20 min baseline (5 mM

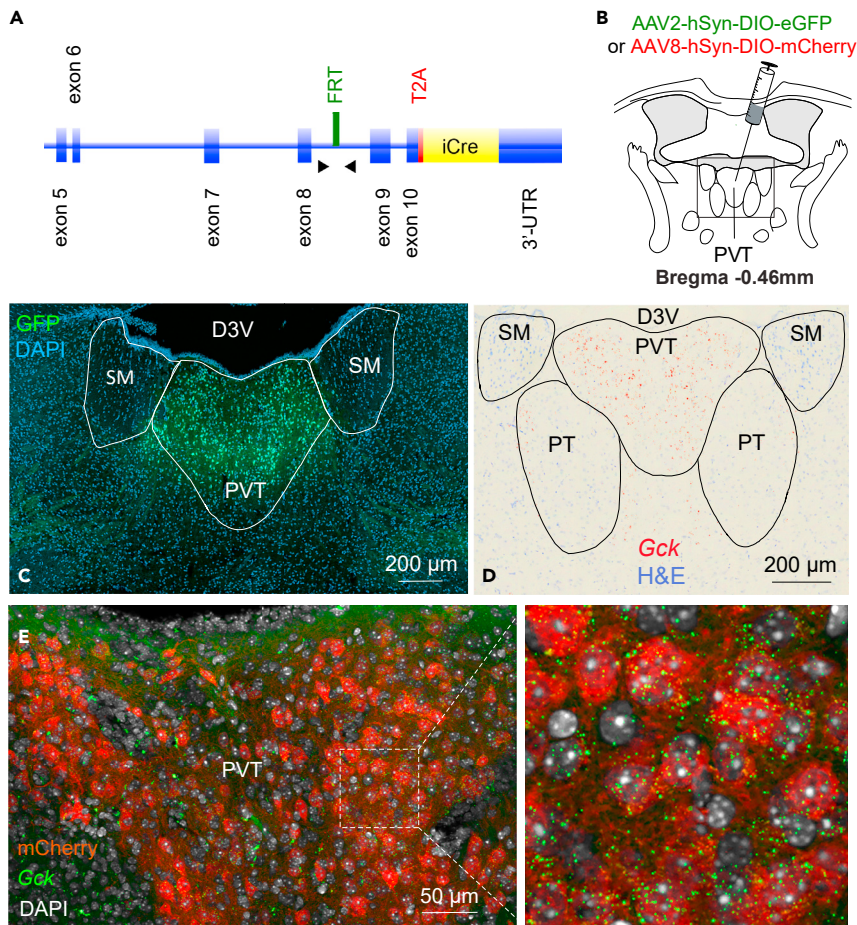


Figure 2. *Gck*^{cre/+} mice and *Gck*^{aPVT} neurons

(A) Scheme of the modified *Gck*^{Cre} allele with insertion of the T2A and iCre sequence just before the *Gck* STOP signal in exon10. The location of the primers for genotyping is indicated by arrowheads. *FRT*: flippase recognition target; *T2A*: ribosomal skipping sequence.

(B) An AAV2-*hSyn-DIO-eGFP* or AAV8-*hSyn-DIO-mCherry* were injected in the PVT of *Gck*^{cre/+} mice allowing for the Cre-dependent expression of the fluorescent proteins.

(C) *Gck* neurons labeled with eGFP in a brain coronal section.

(D) *In situ* hybridization of *Gck* mRNA (red) and hematoxylin/eosin staining (H&E; purple).

(E) Fluorescent *in situ* hybridization detection of *Gck* mRNA (green) and of mCherry (red). *D3V*: dorsal 3rd ventricle, *PVT*: paraventricular thalamic nucleus, *PT*: paratenial thalamic nucleus, *SM*: stria medullaris.

glucose), neurons were superfused with solutions containing 3.5 mM, 2 mM and 0.5 mM glucose (7 min each). Between each test solution, brain slices were superfused with the 5 mM glucose solution. Overall, 54% of the neurons tested were GE (Figures 4D and 4E) while 21% were GI (Figures 4D and 4F) and 25% were NR neurons (Figures 4D and 4G). GE neurons showed a significant, reversible decrease in their membrane potential at 0.5 mM glucose (Gaussian GLMM-PQL: $t = 5.7$, adj. $p < 0.001$ and $t = 8.4$, adj. $p < 0.001$; Figure 4H) along with a reduction in their spike frequency (Poisson GLMM-PQL: $t = 4.3$, adj. $p < 0.001$ and $t = 4.4$, adj. $p < 0.001$; Figure 4J), whereas GI neurons exhibited reversible depolarization (Gaussian GLMM-PQL: $t = -2.6$, adj. $p < 0.05$ and $t = -2.7$, adj. $p < 0.05$; Figure 4H), and increased spike frequency in the presence of the low glucose concentration (Poisson GLMM-PQL: $t = -2.6$, adj. $p < 0.05$ and $t = -2.4$, adj. $p < 0.05$; Figure 4J). NR neurons were characterized by the absence of significant changes in membrane potential (Gaussian GLMM-PQL: $t = 0.01$, adj. $p = 0.99$ and $t = 1.9$, adj. $p = 0.16$; Figure 4H) and the spike frequency (Poisson GLMM-PQL: $t = -0.4$, adj. $p = 0.70$, $t = -1.6$, adj. $p = 0.26$; Figure 4J). The glucose dose-dependent hyperpolarization and reduction of firing activity of GE neurons was significant only at 0.5 mM glucose, whereas GI neurons depolarization became significant already at 2 mM glucose (Figures 4I and 4K).

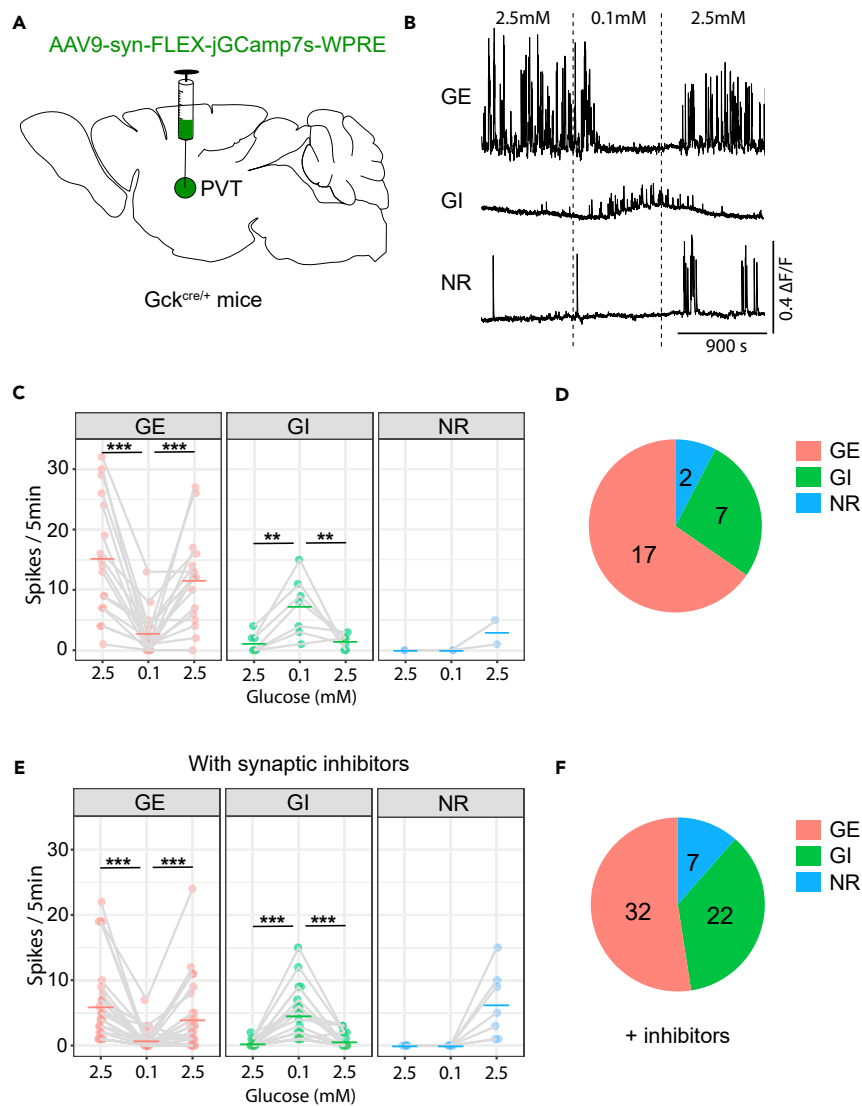


Figure 3. Calcium imaging of Gck^{aPVT} neurons

(A) An AAV9-syn-FLEX-jGCaMP7s was injected in the aPVT of Gck^{cre/+} mice to allow for the cre-dependent expression of jGCaMP7. Calcium recordings were performed on acute brain slices.

(B) Calcium transient monitoring in Gck^{aPVT} neurons in the presence of the indicated glucose concentrations.

(C) Quantification of the calcium spike frequency in response to the indicated changes in glucose concentrations revealed GE, GI, or NR neurons (Poisson GLMM-PQLs).

(D) Distribution of GE, GI, and NR Gck^{aPVT} neurons according to the calcium activity analysis.

(E) Quantification of the calcium spike frequency in the presence of inhibitors of synaptic transmission (Poisson GLMM-PQLs).

(F) Distribution of GE, GI, and NR Gck^{aPVT} neurons according to the calcium activity analysis in the presence of synaptic inhibitors. Proportion of GE, GI, and NR was not significantly different in the presence or absence of synaptic inhibitors. Proportions were compared using binomial GLMs. *** p < 0.001; ** p < 0.01.

Thus, Gck^{aPVT} neurons constitute a heterogeneous population of glucose responsive neurons with the majority of them being activated by high glucose concentrations (GE neurons).

The temporal coding of the Gck^{aPVT} → NAc projections depends on extracellular glucose concentration

In guinea pigs and rats, thalamic neuron activation generates either a phasic or a tonic firing response depending on their basal membrane potential. At hyperpolarizing potentials, a current pulse induces a

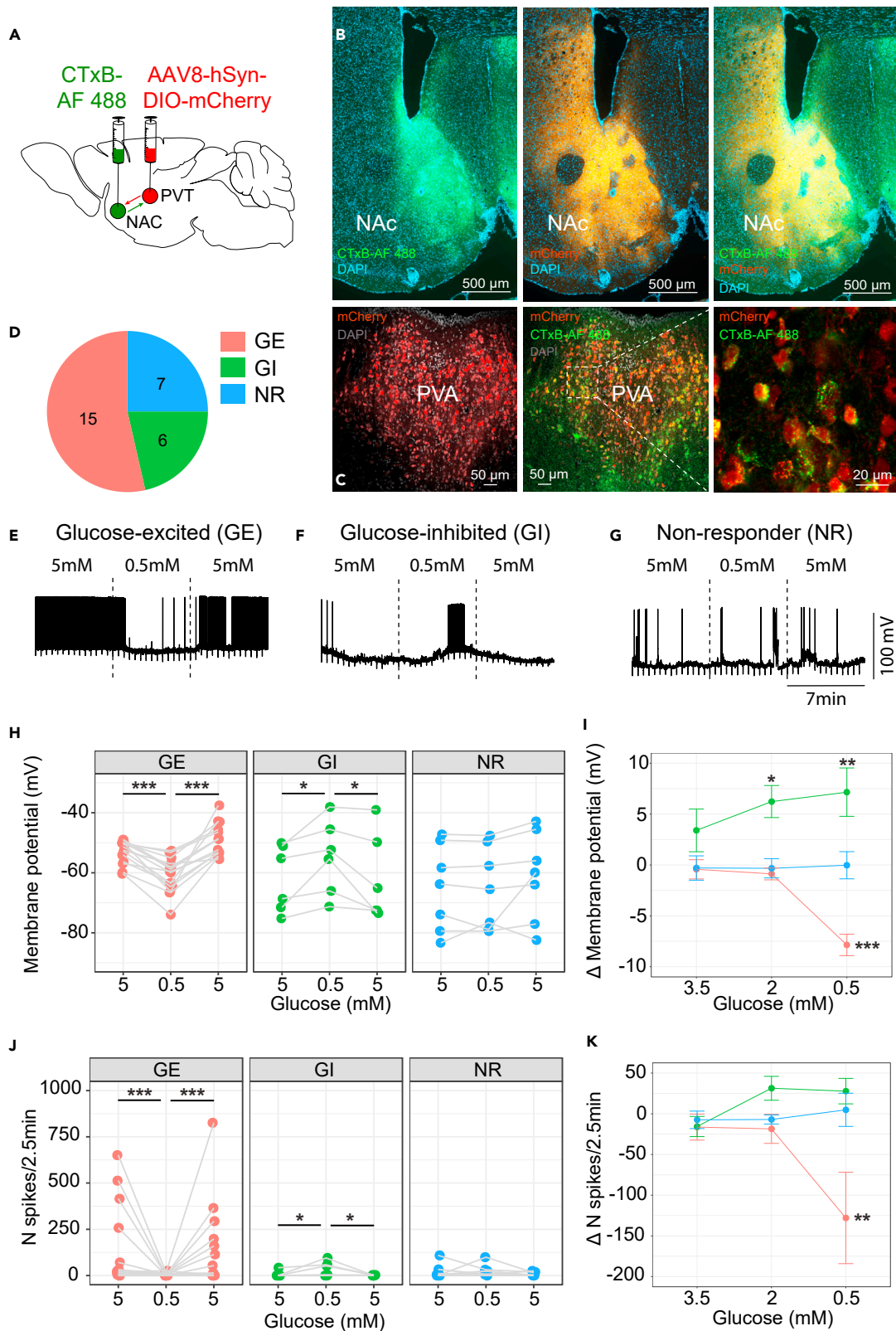


Figure 4. Gck^{aPVT} neurons projecting to the NAc are mostly glucose-excited

Characterization of Gck^{aPVT} neurons projecting to the NAc by whole-cell patch-clamp recordings.

(A) Gck^{cre/+} mice were injected in the aPVT with an AAV8-*hsyn-DIO-mCherry* and with the cholera toxin B subunit-Alexa Fluor 488 conjugate (CTxB-AF 488) bilaterally in the NAc.

(B) Representative images of the NAc showing CTxB (green, left panel), Gck neurons fibers in the core and shell of the NAc (red, middle panel), and the merged image (right panel).

(C) Gck^{aPVT} neurons (red, left) retrogradely labeled from the NAc with CTxB-AF 488 (green, middle). Right panel shows a higher magnification of the doubly labeled Gck^{aPVT} neurons. Images in B and C were taken from the same animal.

(D) Proportion of GE, GI and NR Gck^{aPVT} neurons determined by patch-clamp analysis in the presence of the indicated glucose concentrations.

(E–G) Representative traces of a GE (D), a GI (E) and a NR neuron (F) in response to the indicated glucose concentrations.

(H–K) Quantification of changes in membrane potential (H and I) and spike frequency (J and K). Statistical differences were analyzed using Gaussian GLMM-PQLs for membrane potentials (H) and Poisson GLMM-PQLs for firing activity (J). Statistical differences between delta values of the membrane potential (I) and the spike frequency (K) were both investigated with Gaussian GLMM-PQLs. Graphs show means \pm s.e.m. *** $p < 0.001$; ** $p < 0.01$; * $p < 0.05$.

bursting firing response, whereas the same current pulse induces a tonic response when the neurons are depolarized above -60 mV (Kolaj et al., 2007; Linás and Jahnsen, 1982). Here, we first verified that NAc-projecting Gck^{aPVT} neurons displayed the same profile. The injection of a depolarizing current ($+70$ pA) indeed switched the response from a tonic to a phasic pattern after the artificial hyperpolarization of these neurons below -65 mV (Figures 5A and 5B). The fast and slow spiking components of the rebound after a -200 pA hyperpolarizing step were dependent on a Na⁺ and a Ca²⁺ conductance, respectively, as TTX inhibited the fast spiking in a hyperpolarized (< -65 mV) neuron (Figures 5C and 5D) and the Ca²⁺-dependent slow spiking component was inhibited by replacing Ca²⁺ by Mg²⁺ in the presence of the Ca²⁺ channel blocker CoCl₂ (Figure 5E). After washout of the ion channels inhibitors, both fast and slow spiking components of the rebound induced by the hyperpolarizing step were restored (Figure 5F).

We then assessed whether the firing mode of the NAc-projecting Gck^{aPVT} GE neurons was modified by external glucose concentrations. We found that at 5 mM glucose, Gck^{aPVT} GE neurons generated fast Na⁺ spikes characteristic of tonic firing in response to a -20 pA hyperpolarizing current injection (Figure 5G). This response was characteristic of a tonic pattern devoid of the Ca²⁺-dependent slow component observed in bursts. However, at 0.5 mM glucose, when these neurons were hyperpolarized, the same current injection generated an additional slow Ca²⁺ spike (low threshold spikes, LTS) together with multiple fast Na⁺ spikes (burst firing, Figure 5H). Analysis of the Gck^{aPVT} GE neurons recordings of Figure 4 revealed a reciprocal change in firing modes when the extracellular glucose concentrations were shifted from 5 mM to 0.5 mM (Figure 5I). This data also showed that at 5 mM glucose, the membrane potentials of Gck^{aPVT} GE, GI and NR neurons showing burst firing were significantly more hyperpolarized (-60.4 ± 2.8 mV) than the neurons showing tonic firing (-53.6 ± 1.7 mV; Wilcoxon-Mann-Whitney test, $W = 21$, $p = 0.03$; Figure 5J). Thus, GE neurons adopt a tonic firing pattern at 5 mM glucose, and a burst pattern at 0.5 mM glucose.

Gck^{aPVT} neurons send excitatory glutamatergic projections to the NAc shell

The Gck^{aPVT} neurons expressed the glutamate presynaptic marker *Vglut2* (*Slc17a6*) (Figure 6A), and were negative for the GABAergic marker *Gad67* (Figure 6B), as expected based on previous reports (Barroso-Chinea et al., 2007; Zhu et al., 2016). To functionally confirm the glutamatergic nature of the Gck^{aPVT} neuron connections to the NAc, we injected an AAV2-*EF1 α -DIO-hChR2(H134R)-eYFP* into the aPVT of Gck^{cre/+} mice (Figure 6C) to express the light-sensitive opsin channelrhodopsin-2 (ChR2). Voltage-clamp analysis of medium spiny neurons (MSNs) of the NAc shell showed that light-stimulation of the ChR2-expressing Gck^{aPVT} terminals in acute coronal sections produced robust inward currents (Figure 6E inset). These currents were inhibited by 10 μ M DNQX but not by 50 μ M picrotoxin (Figures 6D and 6E). Thus, we confirmed that Gck^{aPVT} neurons send excitatory glutamatergic projections to the MSNs of the NAc shell.

Chemogenetic inhibition of Gck^{aPVT} neurons increases food intake

To assess whether the Gck^{aPVT} neurons impact food intake, we first injected an AAV8-*hSyn-DIO-hM4D(Gi)-mCherry* in the aPVT of Gck^{cre/+} mice and control littermates (Gck^{+/+}; Figure 7A). Three weeks later, we monitored the amount of food consumed during 24h following an overnight fasting period. The feeding measurements were started 30min after i.p. injection of clozapine, a synthetic ligand of hM4D(Gi) receptor allowing subsequent inhibition of Gck^{aPVT} neurons. We found that inhibition of Gck^{aPVT} neurons increased the cumulative food intake after 6 hours (Gaussian GLMM-PQL: 6–8 hours ($t = -2.8$, adj. $p < 0.05$), 8–10 hours ($t = -2.7$, adj. $p < 0.05$), 10–12 hours ($t = -3.2$, adj. $p < 0.01$) and 12–24 hours ($t = -4.9$, adj. $p < 0.001$)) as shown by the significant interaction occurring between time bins and genotype (Figure 7B).

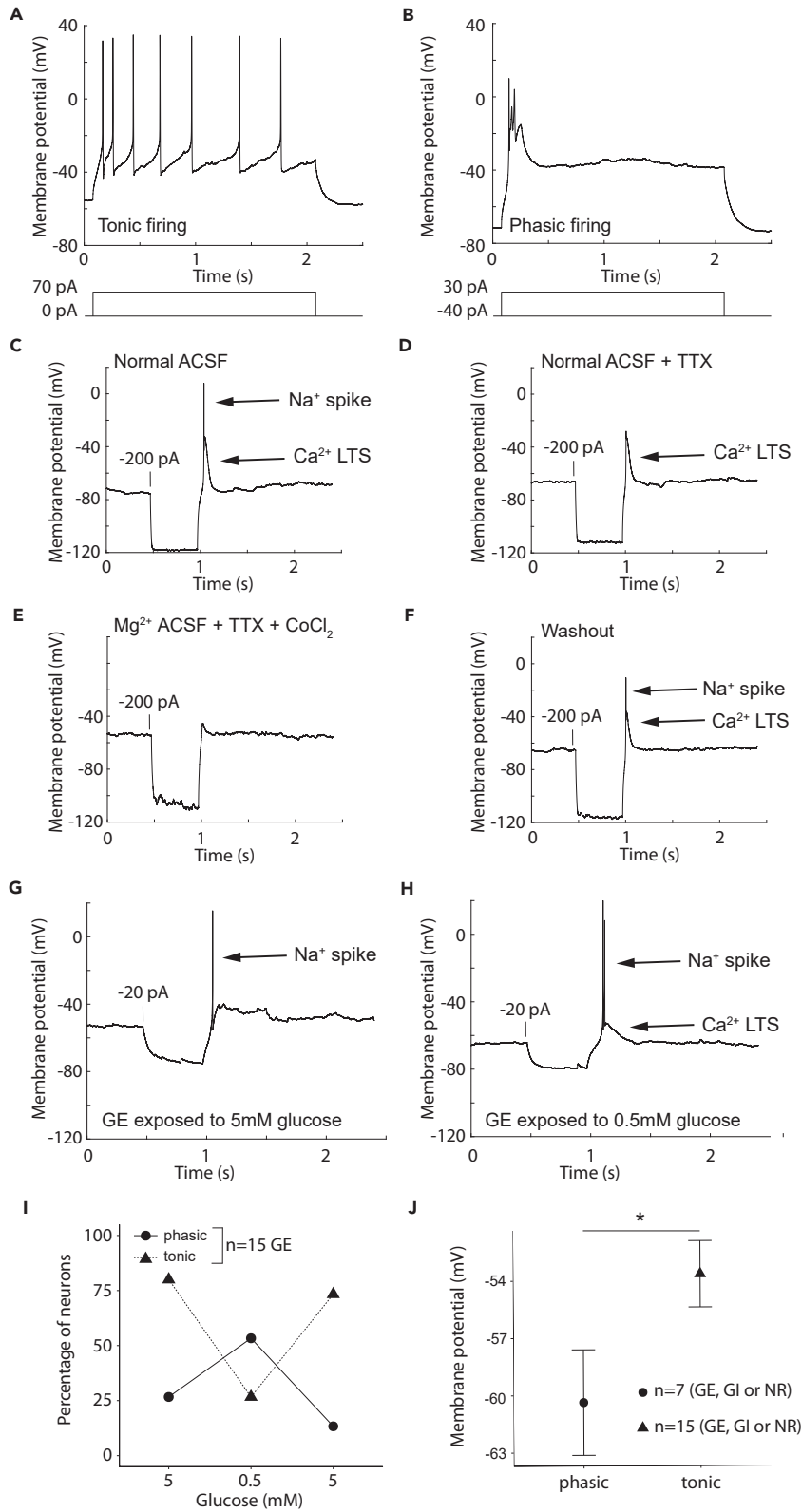


Figure 5. Glucose concentrations change the temporal coding of Gck^{aPVT} neurons

(A) Injection of a depolarizing current induces tonic firing in Gck^{aPVT} neurons maintained at > -60 mV.
(B) Injection of the depolarizing current in the same neuron recorded in (A) and maintained hyperpolarized at < -65 mV induces a phasic response. Recordings in A and B were made in 2.5 mM glucose ACSF.
(C) The rebound spike firing after the injection a hyperpolarizing current in a hyperpolarized (< -65 mV) neuron is characterized by a Na⁺ spike and a low-threshold Ca²⁺ spikes (LTS).
(D) 1 μ M TTX inhibits the fast Na⁺ spikes.
(E) TTX and 1 mM CoCl₂ inhibit the sodium and the calcium component of the spikes respectively.
(F) Restoration of normal rebound spike firing after inhibitors washout. Recordings in C to F are from the same neuron.
(G) At 5 mM glucose, a GE neuron is in a depolarized state and exhibits a tonic firing pattern (Na⁺ spike) following a -20 pA hyperpolarizing step.
(H) At 0.5 mM, the same GE neuron is in a hyperpolarized state and the same hyperpolarizing step elicits a phasic pattern rebound with a sodium spike on top of a slow calcium wave (Ca²⁺ LTS).
(I) A decrease in the glucose concentration from 5 to 0.5 mM leads to a decreased proportion of GE neurons displaying a tonic firing pattern and a reciprocal increase in the number of neurons exhibiting a phasic firing profile. Data are from GE neurons (n = 15) presented in Figure 4.
(J) Among GE, GI, and NR neurons, those displaying phasic firing at 5 mM glucose (n = 7) are significantly more hyperpolarized than the ones showing tonic firing (n = 15). Wilcoxon-Mann-Whitney test was used. Mean values of the membrane potential are from recordings presented in Figure 4 during the last 2.5 min preceding the stimulation with 0.5 mM glucose. Graphs show means \pm s.e.m. *p < 0.05.

Optogenetic activation of Gck^{aPVT} terminals in the NAc decreases sucrose reward seeking

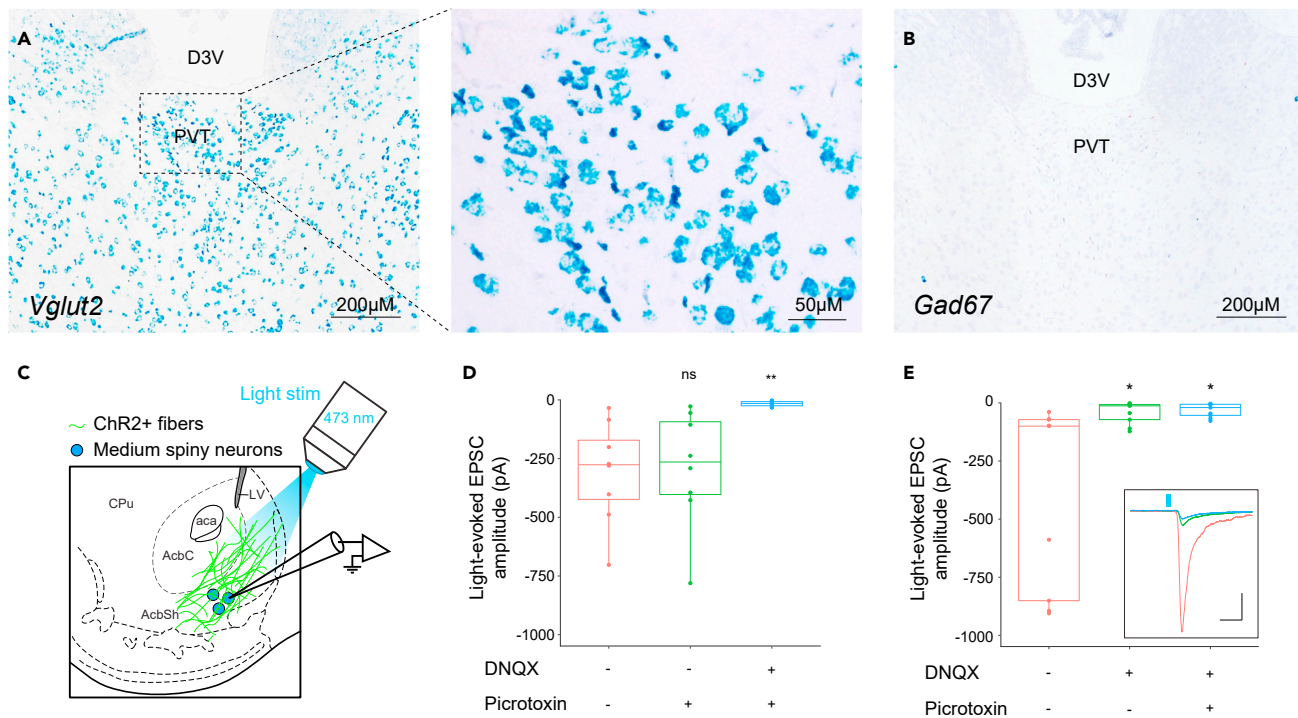
To evaluate the impact of activating Gck^{aPVT} neurons projecting to the NAc on operant conditioning behavior, we injected Gck^{cre/+} and Gck^{+/+} mice in the aPVT with an AAV2-Ef1 α -DIO-hChR2(H134R)-eYFP-WPRE-pA (Figure 7C). An operant conditioning protocol was then performed following implantation of optic fibers bilaterally just above the NAc shell (Figure 7C). *Ad libitum* fed mice were first trained to obtain sucrose reward (10 μ L of a 10% sucrose liquid solution) during 30 min daily sessions for 8 consecutive days using a fixed ratio 1 (FR1) operant conditioning schedule in the absence of light stimulation (data not shown). The number of rewards taken was then quantified during 30 min daily sessions with 20 or 40 Hz light stimulation. The number of rewards obtained between genotypes diverged upon 20 Hz stimulation, but became significant with 40 Hz stimulation at days 8 and 9 (Figures 7D and 7E) when the Gck^{cre/+} mice performed fewer active nosepokes, and obtained fewer rewards (at day 8: Poisson GLMM-PQLs: $t = 3.8$, adj. $p < 0.001$ and $t = 4.1$, adj. $p < 0.001$; for D and E, respectively. At day 9: $t = 3.9$, adj. $p < 0.001$ and $t = 3.9$, adj. $p < 0.001$, for D and E, respectively).

We then subjected the mice to a 90 min daily progressive-ratio (PR) schedule in which the number of nose-pokes required to earn each successive reward was progressively increased. The light stimulation of the ChR2-expressing Gck^{aPVT} terminals in the NAc reduced the number of active nosepokes (2-sided Student's t-test: $t = -2.7$, $df = 16$, * $p < 0.05$; Figure 7F), the numbers of rewards obtained ($t = -3.4$, $df = 16$, ** $p < 0.01$; Figure 7G) and the maximal operant responses (breakpoints; $t = -2.9$, $df = 16$, * $p < 0.05$; Figure 7H). Thus, activation of Gck^{aPVT} neurons projecting to the NAc decreased the mouse motivation to obtain sucrose rewards.

DISCUSSION

Here, by using *in situ* hybridization microscopy analysis and a mouse Gck^{Cre} reporter line, we showed that Gck was widely expressed in neurons of the PVT. By combining *ex vivo* Ca²⁺ imaging and electrophysiological recordings we showed that Gck^{aPVT} neurons projecting to the NAc were mostly glucose excited. Chemogenetic and optogenetics approaches to assess behavioral responses revealed that the Gck^{aPVT} neurons projecting to the NAc negatively control feeding and sucrose seeking behavior. Gck^{aPVT} neurons, thus, display opposite properties to the previously described Glut2^{aPVT} neurons, which are activated by hypoglycaemia, and increase sucrose-seeking behavior (Labouèbe et al., 2016).

The PVT is as an important site of integration of energy homeostasis-related cues with the control of the reward system and motivated-feeding behavior (Hua et al., 2018; Kelley et al., 2005; Millan et al., 2017). This integrative role depends on the innervation of the PVT by afferent connections coming, in particular, from several hypothalamic nuclei, and on efferent projections to the NAc (Kirouac, 2015; Ligorio et al., 2009). PVT neurons are also sensitive to changes in extracellular glucose concentrations as previously demonstrated for Glut2-expressing neurons (Labouèbe et al., 2016). Indeed, Glut2^{aPVT} neurons are



activated by hypoglycemia (GI neurons), and when activated, they increase sucrose-seeking behavior through their glutamatergic projections to the NAc. *Glut2* neurons form a relatively small subpopulation of cells in the PVT, in contrast to the *Gck* neurons which are widely distributed in the anterior and posterior PVT. *Gck^{aPVT}* neurons send dense projections to the NAc to activate MSNs through synaptic glutamate release. Ca^{2+} imaging experiments using the genetically-encoded Ca^{2+} indicator GCaMP7, revealed that approximately two-thirds of the *Gck^{aPVT}* neurons are activated by hyperglycemia (GE neurons), and the rest being equally divided in GI and NR neurons. When synaptic transmission was inhibited GE and GI neurons were still detected, indicating that their glucose responsiveness is cell autonomous. Patch-clamp analysis confirmed that *Gck^{aPVT}* neurons projecting to the NAc consist of GE, GI and NR neurons in the same proportion as found by Ca^{2+} imaging. An interesting observation of the patch clamp experiments was that the temporal firing pattern of these *Gck* neurons, tonic vs. phasic, was dependent on their membrane potential. This is in accordance with previous studies (Kolaj et al., 2007; Llinás and Jahnsen, 1982) but, here, we further describe that the GE neurons excitability is glucose-dependent and determine their firing mode. In particular, we found that in the presence of 5 mM glucose GE neurons, which are in their most depolarized state, display a clear shift towards a tonic firing mode while a phasic/burst mode was observed under hypoglycemic conditions. This tonic-to-phasic switch in firing pattern may allow *Gck^{aPVT}* GE neurons to encode for different behavioral outputs depending on glucose availability. Indeed, tonic versus phasic transmission onto the same targets triggers divergent behavioral outcomes notably on motivated behavior (Budygin et al., 2020) and cue-associated learning (Ellwood et al., 2017).

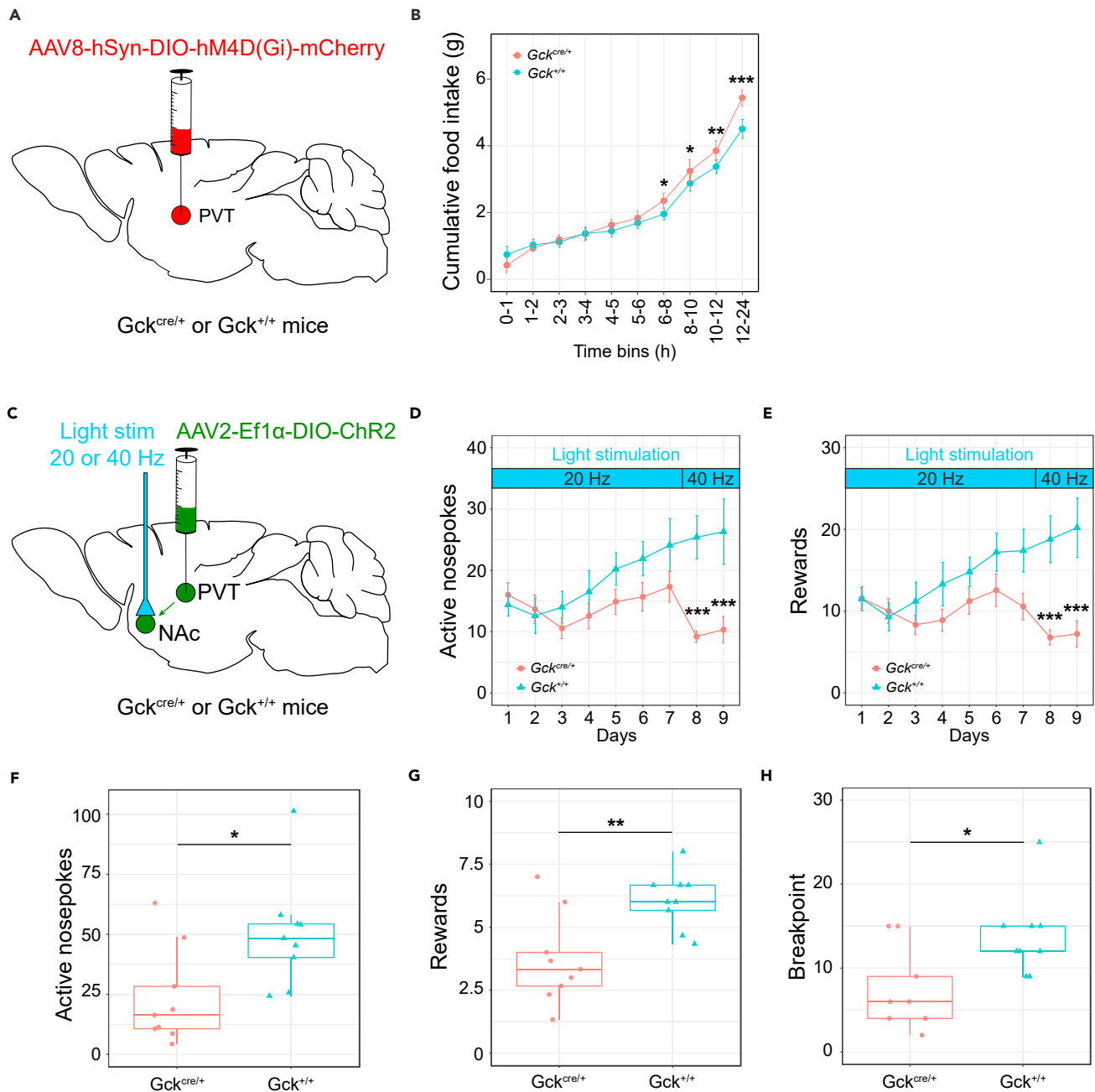


Figure 7. Gck^{aPVT} neurons control feeding and motivated sucrose seeking

(A) $Gck^{cre/+}$ ($n = 8$) and $Gck^{+/+}$ ($n = 7$) littermate mice were injected in the aPVT with an AAV8-hSyn-DIO-hM4D(Gi)-mCherry.

(B) I.p. injection of clozapine in hM4Di-expressing mice induced higher food intake as measured over a 24-hour period. A significant interaction between the genotypes and the time bins affects the food intake after 6 hours (Gaussian GLMM-PQL). Graphs show means \pm s.e.m. *** $p < 0.001$; ** $p < 0.01$; * $p < 0.05$.

(C) $Gck^{cre/+}$ and $Gck^{+/+}$ littermate mice were injected in the aPVT with an AAV2-Ef1 α -DIO-hChR2(H134R)-eYFP-WPRE-pA. Gck neuronal projections were stimulated by 10 ms blue light pulses delivered bilaterally into the NAc shell (20 Hz or 40 Hz; 1 s on/1 s off; 10–15 mW).

(D and E) Fixed ratio conditioning for sucrose in fed $Gck^{cre/+}$ ($n = 9$) or $Gck^{+/+}$ ($n = 10$) mice during 30 min daily sessions with light stimulation at the indicated frequencies. Number of active nosepokes performed (D) or rewards obtained (E) during those daily sessions. A Poisson GLMM-PQL was used.

(F–H) Under a progressive ratio schedule, light stimulation of Gck^{aPVT} terminals in NAc evoked a decrease in the number of active nosepokes, of sucrose rewards and in the breakpoint values. A 2-sided Student's t-test was used. Graphs show means \pm s.e.m; boxplots represent the medians, the 25–75% interquartile range (IQR) intervals (boxes), the lowest and the highest data points still within 1.5 of the IQR range. *** $p < 0.001$; ** $p < 0.01$; * $p < 0.05$.

In behavioral studies performed upon chemogenetic inhibition or optogenetic activation of the Gck^{aPVT} neurons, we found that these neurons play a role in feeding and motivated-sucrose seeking. Indeed, Gck^{aPVT} neurons chemogenetic inhibition increased feeding when measured over a 24-hour period. In contrast, their acute optogenetic activation in operant conditioning experiments markedly reduced motivated sucrose seeking. These observations are in line with previous publications showing that PVT \rightarrow NAc projections drive feeding inhibition and behavioral aversion (Do-Monte et al., 2017; Hua et al., 2018; Lafferty et al., 2020; Zhu et al., 2016). However, it has to be noted that Gck^{aPVT} neurons project to several brain structures in addition to the NAc, such as the amygdala and the prefrontal cortex (Gaspari S., Quenneville S., Rodriguez-Sanchez-Archidona A., Thorens B., Croizier S., in preparation), which are also involved in various aspects of feeding behavior. Also, optogenetic activation of Gck^{aPVT} terminals in the NAc may induce back-propagation and activate collaterals that innervate other structures. Thus, although we propose that the impact on feeding behavior of modulating the activity of Gck^{aPVT} neurons depends on their projections to the NAc, we cannot exclude the involvement of other brain structures in determining the assessed behavior. Other observations (Cheng et al., 2018), however, reported that activation of the PVT \rightarrow NAc circuit significantly increased food consumption in a novelty-suppressed feeding paradigm. These conflicting results may reflect the presence of different neuronal populations within the PVT. This is supported by our previous study which showed that $Glut2^{aPVT}$ neurons form a homogenous population of GI neurons which, when activated by hypoglycemia, by selective *Glut2* gene inactivation, or by optogenetics, increases sucrose-seeking behavior (Labouèbe et al., 2016).

An intriguing but yet unanswered question is why activation of $Glut2^{aPVT}$ neurons by hypoglycemia and Gck^{aPVT} neurons by hyperglycemia leads to opposite effects on feeding behavior when both types of neurons activate MSN NAc neurons by glutamatergic connections. One possibility is that the activation of MSNs and their behavioral outputs may be differentially affected by hypoglycemia or hyperglycemia through signals generated by other glucose sensing cells interacting with the reward system. Alternatively, the temporal coding of the Gck^{aPVT} neurons, which differs between high and low glucose concentrations, may have differential effect on MSNs. Still another possibility is that these different neurons may make selective connections to MSNs expressing either the dopamine receptor D1R or D2R, which could elicit opposite behavioral outcomes despite similar activity patterns (Cox and Witten, 2019). However, in this and our previous (Labouèbe et al., 2016) studies, all the MSNs we recorded were activated by optogenetic activation of Gck^{aPVT} or $Glut2^{aPVT}$ neurons, suggesting the absence of selective projections to either D1R or D2R expressing MSNs. More work is needed to understand the differential effect of activating MSN neurons by $Glut2^{aPVT}$ or Gck^{aPVT} neurons.

An interesting observation is that activation of $Glut2^{aPVT}$ and Gck^{aPVT} neurons leads to opposite control over motivated feeding, suggesting that they represent separate PVT neuronal subpopulations. We previously found that activation of $Glut2^{aPVT}$ neurons by hypoglycemia was suppressed when extracellular glucose concentrations were raised and that *Glut2* inactivation prevented this silencing. We made similar observations with the *Glut2* neurons of the nucleus of the tractus solitarius ($Glut2^{NTS}$), which were activated by neuroglucopenia and silenced by the presence of high glucose concentrations in the patch pipet (Lamy et al., 2014). Thus, *Glut2* seems to be required to allow efficient glucose uptake when glycemia rise back to normal levels to restore cellular energy and suppress firing activity. The role of *Gck* in glucose sensing is less clear. Indeed, *Gck* is present in GE, GI, and NR neurons of the PVT and of the VMN (Steinbusch et al., 2016). *Gck* expression may, thus, not be required for neuronal glucose sensing. Indeed, in a previous study, we inactivated *Gck* in *Sf1* neurons of the VMN and found that the glucose sensing properties of GE or GI neurons remained intact. We nevertheless, observed that female, but not male mice displayed increased fat mass and a defect in hypoglycemia-induced glucagon secretion (Steinbusch et al., 2016). Thus, *Glut2* and *Gck*, which cooperate for efficient glucose signaling to insulin secretion in beta-cells, characterize cell populations in the thalamus, which have different properties and physiological functions. It is, however, not known whether $Glut2^{aPVT}$ neurons represent the subpopulation of GI Gck^{aPVT} neurons or a distinct neuronal population. In addition, the role of *Gck* expression in PVT neurons in gluco-regulation and feeding behavior is still undefined.

In summary, we identified a subpopulation of cells in the PVT, the Gck^{aPVT} neurons, and established that, although they have different glucose sensitivities, the majority of them are activated by a rise in glucose concentrations. We found that their inhibition increases feeding whereas their activation suppresses glucose seeking behavior. Together with our previous study on $Glut2^{aPVT}$ neurons, this establishes the

presence of two cell populations in the PVT, with opposite glucose sensing properties and role on feeding behavior, and provides a genetic basis and a mouse model to distinguish these cell populations. Together our results provide new information and tools to support future studies aimed to understand the role of the thalamus in integrating enteroceptive, energy-related signals with feeding behavior.

Limitation of the study

One limitation in our study is that despite Gck^{aPVT} neurons are in majority GE neurons, they also include GI and NR neurons but our chemogenetic and optogenetic experiments test the impact of inhibiting/activating the whole population. Specifically, targeting each neuronal subpopulation independently may have opposing effect on the feeding behavior. Also, whether $Glut2^{aPVT}$ neurons, which form a homogenous population of GI neurons suppressing sucrose seeking behavior, also express glucokinase remains to be characterized.

STAR★METHODS

Detailed methods are provided in the online version of this paper and include the following:

- KEY RESOURCE TABLE
- RESOURCE AVAILABILITY
 - Lead contact
 - Materials availability
 - Data and code availability
- EXPERIMENTAL MODEL DETAILS
- METHOD DETAILS
 - Genotyping
 - Stereotaxy
 - *In situ* hybridization and image acquisition
 - Identification of Gck^{aPVT} neurons projecting to the NAc
 - Ex-vivo calcium imaging
 - Ex-vivo patch-clamp experiments
 - *In vivo* chemogenetics
 - *In vivo* optogenetics
- QUANTIFICATION AND STATISTICAL ANALYSIS
 - Quantification of the calcium transients from the ex-vivo calcium imaging experiments
 - Current-clamp mode recordings analysis
 - Ex-vivo recordings in voltage-clamp mode
 - Statistical analysis

ACKNOWLEDGMENTS

The present work was supported by a European Research Council Advanced Grant (INTEGRATE, No. 694798) and a Swiss National Science Foundation grant (310030-182496) to BT.

AUTHOR CONTRIBUTIONS

B.T., G.L., S.C., S.K., and S.G. conceived the experiments. S.K., G.L., S.C., S.G., and D.T. performed the experiments. S.K., G.L., S.C., S.G., and B.T. analyzed the data. S.K., G.L. and B.T. wrote the first draft of the manuscript. All authors critically read the manuscript.

DECLARATION OF INTERESTS

The authors declare no competing interests.

Received: May 20, 2021

Revised: July 8, 2021

Accepted: September 9, 2021

Published: October 22, 2021

REFERENCES

- Ashcroft, F.M., and Rorsman, P. (2012). Diabetes mellitus and the beta cell: the last ten years. *Cell* 148, 1160–1171. [10.1016/j.cell.2012.02.010](https://doi.org/10.1016/j.cell.2012.02.010).
- Barroso-Chinea, P., Castle, M., Aymerich, M.S., Pérez-Manso, M., Erro, E., Tuñón, T., and Lanciego, J.L. (2007). Expression of the mRNAs encoding for the vesicular glutamate transporters 1 and 2 in the rat thalamus. *J. Comp. Neurol.* 501, 703–715.
- Bentsen, M.A., Mirzadeh, Z., and Schwartz, M.W. (2019). Revisiting how the brain senses glucose—and why. *Cell Metab* 29, 11–17. Epub 2018 Dec 10. [10.1016/j.cmet.2018.10.111](https://doi.org/10.1016/j.cmet.2018.10.111).
- Berridge, K.C., and Robinson, T.E. (1998). What is the role of dopamine in reward: hedonic impact, reward learning, or incentive salience? *Brain Res. Brain Res. Rev.* 28, 309–369.
- Brüning, J.C., Gautam, D., Burks, D.J., Gillette, J., Schubert, M., Orban, P.C., Klein, R., Krone, W., Müller-Wieland, D., and Kahn, C.R. (2000). Role of brain insulin receptor in control of body weight and reproduction. *Science* 289, 2122–2125.
- Budygin, E.A., Bass, C.E., Grinevich, V.P., Deal, A.L., Bonin, K.D., and Weiner, J.L. (2020). Opposite consequences of tonic and phasic increases in accumbens dopamine on alcohol-seeking behavior. *iScience* 23, 100877.
- Cheng, J., Wang, J., Ma, X., Ullah, R., Shen, Y., and Zhou, Y.D. (2018). Anterior paraventricular thalamus to nucleus accumbens projection is involved in feeding behavior in a novel environment. *Front Mol. Neurosci.* 11, 202.
- Cox, J., and Witten, I.B. (2019). Striatal circuits for reward learning and decision-making. *Nat. Rev. Neurosci.* 20, 482–494.
- Dana, H., Sun, Y., Mohar, B., Hulse, B.K., Kerlin, A.M., Hasseman, J.P., Tsegaye, G., Tsang, A., Wong, A., Patel, R., et al. (2019). High-performance calcium sensors for imaging activity in neuronal populations and microcompartments. *Nat. Methods* 16, 649–657.
- de Felipe, P., Hughes, L.E., Ryan, M.D., and Brown, J.D. (2003). Co-translational, intraribosomal cleavage of polypeptides by the foot-and-mouth disease virus 2A peptide. *J. Biol. Chem.* 278, 11441–11448. [10.1074/jbc.M211644200](https://doi.org/10.1074/jbc.M211644200).
- Do-Monte, F.H., Minier-Toribio, A., Quinones-Laracuente, K., Medina-Colon, E.M., and Quirk, G.J. (2017). Thalamic regulation of sucrose seeking during unexpected reward omission. *Neuron* 94, 388–400. [10.1016/j.neuron.2017.03.036](https://doi.org/10.1016/j.neuron.2017.03.036).
- Ellwood, I.T., Patel, T., Wadia, V., Lee, A.T., Liptak, A.T., Bender, K.J., and Sohal, V.S. (2017). Tonic or phasic stimulation of dopaminergic projections to prefrontal cortex causes mice to maintain or deviate from previously learned behavioral strategies. *J. Neurosci.* 37, 8315–8329.
- Hirschberg, P.R., Sarkar, P., Teegala, S.B., and Routh, V.H. (2020). Ventromedial hypothalamus glucose-inhibited neurons: a role in glucose and energy homeostasis? *J. Neuroendocrinol* 32, e12773.
- Hua, R., Wang, X., Chen, X., Wang, X., Huang, P., Li, P., Mei, W., and Li, H. (2018). Calretinin neurons in the midline thalamus modulate starvation-induced arousal. *Curr. Biol.* 28, 3948–3959. [e3944](https://doi.org/10.1016/j.cub.2018.08.044).
- Kang, L., Dunn-Meynell, A.A., Routh, V.H., Gaspers, L.D., Nagata, Y., Nishimura, T., Eiki, J., Zhang, B.B., and Levin, B.E. (2006). Glucokinase is a critical regulator of ventromedial hypothalamic neuronal glucosensing. *Diabetes* 55, 412–420.
- Kelley, A.E., Baldo, B.A., and Pratt, W.E. (2005). A proposed hypothalamic-thalamic-striatal axis for the integration of energy balance, arousal, and food reward. *J. Comp. Neurol.* 493, 72–85.
- Kirouac, G.J. (2015). Placing the paraventricular nucleus of the thalamus within the brain circuits that control behavior. *Neurosci. Biobehav. Rev.* 56, 315–329.
- Kolaj, M., Doroshenko, P., Yan Cao, X., Coderre, E., and Renaud, L.P. (2007). Orexin-induced modulation of state-dependent intrinsic properties in thalamic paraventricular nucleus neurons attenuates action potential patterning and frequency. *Neuroscience* 147, 1066–1075.
- Kurita, H., Xu, K.Y., Maejima, Y., Nakata, M., Dezaki, K., Santoso, P., Yang, Y., Arai, T., Gantulga, D., Muroya, S., et al. (2015). Arcuate Na⁺/K⁺-ATPase senses systemic energy states and regulates feeding behavior through glucose-inhibited neurons. *Am. J. Physiol. Endocrinol. Metab.* 309, E320–E333.
- Labouèbe, G., Boutrel, B., Tarussio, D., and Thorens, B. (2016). Glucose-responsive neurons of the paraventricular thalamus control sucrose-seeking behavior. *Nat. Neurosci.* 19, 999–1002. [10.1038/nn.4331](https://doi.org/10.1038/nn.4331).
- Lafferty, C.K., Yang, A.K., Mendoza, J.A., and Britt, J.P. (2020). Nucleus accumbens cell type- and input-specific suppression of unproductive reward seeking. *Cell Rep* 30, 3729–3742. [e3723](https://doi.org/10.1016/j.celrep.2020.03.023).
- Lamy, C.M., Sanno, H., Labouèbe, G., Picard, A., Magnan, C., Chatton, J.Y., and Thorens, B. (2014). Hypoglycemia-activated GLUT2 neurons of the nucleus tractus solitarius stimulate vagal activity and glucagon secretion. *Cell Metab* 19, 527–538. [10.1016/j.cmet.2014.02.003](https://doi.org/10.1016/j.cmet.2014.02.003).
- Ligorio, M., Descarries, L., and Warren, R.A. (2009). Cholinergic innervation and thalamic input in rat nucleus accumbens. *J. Chem. Neuroanat.* 37, 33–45.
- Llinás, R., and Jahnsen, H. (1982). Electrophysiology of mammalian thalamic neurones in vitro. *Nature* 297, 406–408.
- Marty, N., Dallaporta, M., and Thorens, B. (2007). Brain glucose sensing, counterregulation, and energy homeostasis. *Physiology (Bethesda)* 22, 241–251.
- Millan, E.Z., Ong, Z., and McNally, G.P. (2017). Paraventricular thalamus: gateway to feeding, appetitive motivation, and drug addiction. *Prog. Brain Res.* 235, 113–137. [10.1016/bs.pbr.2017.07.006](https://doi.org/10.1016/bs.pbr.2017.07.006).
- Novelle, M.G., and Diéguez, C. (2018). Food addiction and binge eating: lessons learned from animal models. *Nutrients* 10, 71. <https://doi.org/10.3390/nu10010071>.
- Pinheiro, J., Bates, D., DebRoy, S., and Sarkar, D.; R Core Team (2018). {nlme}: Linear and Nonlinear Mixed Effects Models.
- Quenneville, S., Labouèbe, G., Basco, D., Metref, S., Viollet, B., Foretz, M., and Thorens, B. (2020). Hypoglycemia-sensing neurons of the ventromedial hypothalamus require AMPK-induced Txn2 expression but are dispensable for physiological counterregulation. *Diabetes* 69, 2253–2266.
- R Core Team (2018). A Language and Environment for Statistical Computing (R Foundation for Statistical Computing).
- Richardson, N.R., and Roberts, D.C. (1996). Progressive ratio schedules in drug self-administration studies in rats: a method to evaluate reinforcing efficacy. *J Neurosci Methods.* [https://doi.org/10.1016/0165-0270\(95\)00153-0](https://doi.org/10.1016/0165-0270(95)00153-0).
- Saltiel, A.R., and Kahn, C.R. (2001). Insulin signalling and the regulation of glucose and lipid metabolism. *Nature* 414, 799–806.
- Shimshek, D.R., Kim, J., Hübner, M.R., Spergel, D.J., Buchholz, F., Casanova, E., Stewart, A.F., Seeburg, P.H., and Sprengel, R. (2002). Codon-improved Cre recombinase (iCre) expression in the mouse. *Genesis* 32, 19–26.
- Silver, I.A., and Erecinska, M. (1998). Glucose-induced intracellular ion changes in sugar-sensitive hypothalamic neurons. *J. Neurophysiol.* 79, 1733–1745.
- Steinbusch, L., Labouèbe, G., and Thorens, B. (2015). Brain glucose sensing in homeostatic and hedonic regulation. *Trends Endocrinol. Metab.* 26, 455–466. [10.1016/j.tem.2015.06.005](https://doi.org/10.1016/j.tem.2015.06.005).
- Steinbusch, L.K., Picard, A., Bonnet, M.S., Basco, D., Labouèbe, G., and Thorens, B. (2016). Sex-specific control of fat mass and counterregulation by hypothalamic glucokinase. *Diabetes* 65, 2920–2931. [10.2337/db15-1514](https://doi.org/10.2337/db15-1514).
- Thorens, B. (2012). Sensing of glucose in the brain. *Handb Exp. Pharmacol.* 209, 277–294. [10.1007/978-3-642-24716-3_12](https://doi.org/10.1007/978-3-642-24716-3_12).
- Venables, W.N., and Ripley, B.D. (2002). *Modern Applied Statistics with S* (Springer).
- Verberne, A.J., Sabetghadam, A., and Korim, W.S. (2014). Neural pathways that control the glucose counterregulatory response. *Front Neurosci.* 8, 38. [10.3389/fnins.2014.00038](https://doi.org/10.3389/fnins.2014.00038).
- Wickham, H. (2016). *ggplot2: Elegant Graphics for Data Analysis* (Springer-Verlag).
- Zhu, Y., Wienecke, C.F., Nachtrab, G., and Chen, X. (2016). A thalamic input to the nucleus accumbens mediates opiate dependence. *Nature* 530, 219–222.

STAR★METHODS

KEY RESOURCE TABLE

REAGENT or RESOURCE	SOURCE	IDENTIFIER
Bacterial and virus strains		
AAV2-hSyn-DIO-eGFP	Addgene	Cat#50457-AAV2
AAV2-Ef1α-DIO-hChR2(H134R)-eYFP-WPRE-pA	UNC Vector Core	N/A
AAV8-hSyn-DIO-mCherry	Addgene	Cat#50459-AAV8
AAV8-hSyn-DIO-hM4D(Gi)-mCherry	Addgene	Cat#44362-AAV8
AAV9-syn-FLEX-jGCamps7s-WPRE	Addgene	Cat#104491-AAV9
Chemicals, peptides, and recombinant proteins		
Aquatex mounting medium	Sigma-Aldrich	Cat#108562
Cholera Toxin Subunit B, Alexa Fluor™ 488 Conjugate	ThermoFisher Scientific	Cat#C-22841
Clozapine	Sigma-Aldrich	Cat#C6305
Cobalt(II) chloride	Sigma-Aldrich	Cat#232696
DABCO (1,4-Diazabicyclo2.2.2octane)	Sigma-Aldrich	Cat#D27802
DAPI-fluoromount-G®	SouthernBiotech®	Cat#0100-20
DAPI ready-made solution	Sigma-Aldrich	Cat#MBD0015
DL-AP5 Sodium salt	Tocris	Cat#3693
DNQX disodium salt	Tocris	Cat#2312
Mowiol® 4-88	Sigma-Aldrich	Cat#81381
Tris Base	Sigma-Aldrich	Cat#648310
Picrotoxin	Tocris	Cat#1128
Strychnine	Sigma-Aldrich	Cat#S0532
Critical commercial assays		
KAPA2G	Sigma-Aldrich	Cat#KK5500
RNAScope® Fluorescent Multiplex Reagent Kit	ACDBio	Cat# 320850
Experimental models: Organisms/strains		
Mouse: C57BL/6NTac-Gcktm2885(T2A-icre) Arte	In-house breeding	N/A
Oligonucleotides		
Primers for mouse genotyping see STAR Methods	This paper	N/A
Recombinant DNA		
Gad67	ACDBio	Cat#400951
Gck	ACDBio	Cat#400971
VGlut2 (Slc17a6)	ACDBio	Cat#319171-C1
Software and algorithms		
Adobe Illustrator 2020	Adobe	https://www.adobe.com
Axon pClamp software 10	Molecular Devices	https://www.moleculardevices.com/
ggplot2	(Wickham, 2016)	https://cran.r-project.org/web/packages/ggplot2/index.html

(Continued on next page)

Continued

REAGENT or RESOURCE	SOURCE	IDENTIFIER
MASS	(Venables and Ripley, 2002)	https://cran.r-project.org/web/packages/MASS/index.html
Matlab R2016a	The MathWorks	https://www.mathworks.com/products/matlab.html
Med-PC® IV	Med Associates, Inc.	https://www.med-associates.com/product/med-pc-v-software-suite/
Med-PC Data Transfer Utility “MPC2XL”	Med Associates, Inc.	https://www.med-associates.com/product/mpc2xl-data-transfer-utility-for-all-med-pc-users/
Nlme	(Pinheiro et al. 2018)	https://cran.r-project.org/web/packages/nlme/index.html
R 3.5.1	R Core Team	https://www.r-project.org/
Visiview® Imaging Software 3.0.3	Visitron Systems GmbH	https://www.visitron.de/products/visiview-software.html
Zen black 2012	Zeiss	https://www.zeiss.com
AxioVision	Zeiss	https://www.zeiss.com
Other		
Amplifier	Molecular Devices	MultiClamp 700B
BioDAQ system	Research Diets, Inc	https://researchdiets.com/biodaq
DAQ system	Molecular Devices	Digidata 1440A analog/digital interface
Electrode puller	Sutter Instrument®	P-97
Intensity Division Mini Cube	Doric Lenses	Cat#DMC_1x2i_VIS_FC
LRS-0473 DPSS Laser System	Laserglow Technologies	Cat#R471003FX
Micromanipulator	Sutter Instrument®	MPC-325
Custom Patch Cables	Doric Lenses	NA
Uncleaved Fiber Optic Cannula	Thorlabs	Cat#CFML-12U
Operant conditioning chambers	Med Associates, Inc.	Cat#MED-307W-B2
Rotary joints	Doric Lenses	FRJ 1x2i_FC_2FC

RESOURCE AVAILABILITY

Lead contact

Further information and requests for resources should be directed to and will be fulfilled by the lead contact, Bernard Thorens (Bernard.Thorens@unil.ch).

Materials availability

The Gck-Cre mouse line can be requested from the lead author and is subject to an MTA with the University of Lausanne.

Data and code availability

Data: All data reported in this paper will be shared by the lead contact upon request.

Code: This paper does not report original code.

EXPERIMENTAL MODEL DETAILS

Gck^{cre/+} mice were generated by TaconicArtemis GmbH (Köln, Germany) on a C57BL/6N background. All mouse controls were littermates. Unless otherwise stated, animals were housed at a maximum of 5 individuals per cage and fed with a standard chow (Diet 3436, Kliba Nafag, Kaiseraugst, Switzerland or SP-150, Safe, Augy, France). Male mice were used in all experiments when 8–14 weeks old; Six 8-12 week-old female mice were also used in electrophysiology experiments. Detailed of the number, age and sex of mice used is

detailed for each type of experiment described in the [Method details](#). Animals used in *ex-vivo* electrophysiology and histology were housed under a 12-h light/dark cycle (lights on at 7 a.m.) while animals used in behavioral experiments (*in vivo* optogenetics and chemogenetics) were housed under a reverse 12-h light/dark cycle (lights off at 7 a.m.). All animal care and experimental procedures were approved by the Service Vétérinaire du Canton de Vaud (Switzerland) under veterinary license numbers VD3340 and VD3184.

METHOD DETAILS

Genotyping

A multiplex PCR amplification of extracted genomic DNA was used to detect the constitutive knock-in allele as well as the wild-type allele in the *Gck^{cre/+}* mouse line. 2.5 μ l of genomic DNA was used as the template together with 10 picomoles of primers (Quality HPSF, ThermoScientific, Waltham, MA, USA) and 0.1 μ l of KAPA2G PCR kit (KK5500, Fast HotStart PCR Kit, with dNTPs, Roche, Basel, Switzerland). The presence of the *Gck^{cre/+}* transgene was detected by the resultant 364 bps PCR product while the wild-type allele produced a 289 bps using the following pair of primers: forward 5'-tat aga gcg tgg tat ggt gag g-3' and reverse 5'-gac tgt ttg gct tct cct gg-3'. Sense and antisense primers surround the short flippase recognition target (FRT) present on the intron between exon 8 and 9 of the glucokinase in *Gck^{cre/+}* mutants. The reactions were carried out in a 25 μ l final volume in a thermocycler (T3000, Biometra Biomedizinische Analytik GmbH, Goettingen, Germany) under the following cycling conditions: 95 °C for 3 min, followed by 35 cycles of 95 °C for 15 seconds, 60 °C for 15 seconds, and 72 °C for 15 seconds, then finally 1 min at 72 °C.

Stereotaxy

Mice were placed on a stereotaxic frame (Stoelting, Wood Dale, IL, USA) under ketamine/xylazine anesthesia. The surface of the skulls was visualized with a digital microscope (DMS 300, Leica Microsystems GmbH, Wetzlar, Germany). AAV constructs or CtxB were infused at a rate of 100 nl/min using a 33-gauge stainless steel injector (Hamilton Company, Reno, NV, USA) and a microsyringe pump controller (Micro4, World Precision Instruments, Sarasota, FL, USA). For the labeling of *Gck* PVT neurons, a volume of 300 nl of the virus were injected into the PVT with the following coordinates: AP -0.35 / ML \pm 0.7 / DV -3.4 mm with a 10° angle to avoid the damage to the superior sagittal sinus. For the retrograde tracing experiments, 400 nl of CtxB were injected bilaterally into the shell of the NAc (AP +1.5 / ML \pm 1.4 / DV -4.4 mm, 10° angle). For *in vivo* optogenetic experiments, the viral vector *AAV2-Ef1 α -DIO-hChR2(H134R)-eYFP-WPRE-pA* was bilaterally infused in PVT (coordinates: AP -0.35 / ML \pm 0.7 / DV -3.4 mm) 3 weeks prior to experiments and optical fiber cannulas (CFML12U, Thorlabs Inc. Newton, NJ, USA) were positioned bilaterally in NAc (AP +1.5 / ML \pm 1.4 / DV -4.4 mm, 10° angle) and fixed to the skull with surgical screws (P1 Technologies, Roanoke, VA, USA), tissue adhesive (VetBondTM; 3MTM, Saint Paul, MN, USA) and dental cement (Paladur; Kulzer GmbH, Hanau, Germany). To prevent hypothermia, mice were placed on a heating pad (37 °C) during and after surgeries and a liquid gel eye drops was used prevent eyes drying (Viscotears®, Bausch & Lomb, Kingston-upon-Thames, UK).

In situ hybridization and image acquisition

For the chromogenic *in situ* hybridization, brain sections containing the PVT of 14-week-old males were prepared using a mouse brain matrix with 1 mm section dividers (CellPoint Scientific, Gaithersburg, MD, USA), fixed for 28 hours in 10% formalin and embedded in paraffin. Five μ m sections were cut with a microtome and single *in situ* hybridization (ISH) for *Gck* (cat. number: 400971) or double *in situ* hybridization for *Slc17a6* (*Vglut2*) and *Gad67* (cat. number: 319171-C1 and 400951-C1) was performed using RNAscope® probes and RNAscope® 2-plex detection kit (ACDBio, Newark, CA, USA). Sections were counterstained with Mayer's hematoxylin and mounted using aquatex mounting medium (cat. number: 363123S, VWR, Radnor, PA, USA) and observed using an Axio Imager D1 (Zeiss, Oberkochen, Germany).

For fluorescent *in situ* hybridization, 14-week-old males were transcardially perfused with 4% PFA and 20 μ m cryosections were prepared. *Gck* mRNAs were detected using RNAscope probes (Cat# 400971-C1) and RNAscope® Fluorescent Multiplex Detection Reagents following manufacturer's instructions. Sections were mounted using DAPI-fluoromount (SouthernBiotech®, Birmingham, AL, USA) solution. Images were acquired on a ZEISS Axio Imager.M2 microscope, equipped with ApoTome.2 and a Camera AxioCam 702 mono using the AxioVision software (Zeiss, Oberkochen, Germany).

Identification of Gck^{aPVT} neurons projecting to the NAc

Gck neurons of the PVT were identified following injection of an AAV8-*hsyn-DIO-mCherry* (300 nl) into the PVT of 8-week-old male $Gck^{cre/+}$ and CTxB was injected bilaterally into the NAc. 6 weeks later, the mice were transcardially perfused with 4% PFA. Coronal cryosections (16 μ m) were counterstained with DAPI and embedded with laboratory-made mounting medium containing Polyvinylalcohol-4-88 (Mowiol® 4-88), glycerol, Tris-base and the anti-bleaching agent 1,4-Diazabicyclo [2.2.2] octane (DABCO). Images were acquired as described above or with a Zeiss LSM 710 Confocal microscope using the Zen black 2012 software.

Ex-vivo calcium imaging

$Gck^{cre/+}$ males (10 to 17 week-old) were injected in the aPVT with an AAV9-*syn-FLEX-jGCaMP7s-WPRE* and 4-11 weeks later were deeply anesthetized with isoflurane (Provet AG, Lyssach, Switzerland), decapitated, and their brains taken out and immediately placed in an ice-cold high glucose artificial cerebrospinal fluid (ACSF) (in mM: 125 NaCl, 2.5 KCl, 1.25 NaH_2PO_4 , 1 $MgCl_2$, 2 $CaCl_2$, 26 $NaHCO_3$, 7.5 sucrose and 10 glucose; 300 ± 5 mOsm) equilibrated with a 95% O_2 / 5% CO_2 gas mix (Carbagas, Gümligen, Switzerland). 250 μ m coronal sections were prepared with a vibratome (VT1000S; Leica Microsystems GmbH, Wetzlar, Germany) and immediately transferred to an oxygenated ACSF solution, maintained at 32°C for at least 1 h before starting the recordings. Experiments were performed using an upright epifluorescence microscope (BX51WI; Olympus, Tokyo, Japan) mounted on a motorized stage coupled to a micromanipulator (MPC-325, Sutter Instrument, Novato, CA, USA) and equipped with a mercury lamp and an Evolve Electron Multiplying CCD (EMCCD) camera (Teledyne Photometrics Technology, Tucson, AZ, USA) and filters allowing the visualization of jGCaMP7s expressing neurons. Brain slices were superfused with extracellular ACSF containing 2.5 or 0.1 mM glucose and illuminated with pulses of blue light (473 nm wavelength, 1 Hz repetition rate, 10ms pulse width) delivered with a high-power collimated blue LED system (M470L2-C1 + LEDD1B; Thorlabs Inc. Newton, NJ, USA). Fluorescence was detected at >515 nm and acquired through a water immersion objective lens (40X, 0.8 numerical aperture) at a rate of 1 Hz with the Visiview® Imaging Software 3.0.3 (Visitron Systems GmbH, Puchheim, Germany). Up to 9 individual neurons were simultaneously analyzed in the field of view. The solutions in the recording chamber were maintained at 32-34°C with an automatic temperature controller (TC-324B, Warner Instrument Corporation, Harvard Bioscience, Holliston, MA, USA) and the flow rate adjusted to ~ 2 ml/min (Ismatec peristaltic pump, ISM832C, Cole-Parmer GmbH, Wertheim, Germany). Fluorescence was measured with the “intensity over time” command of the Visiview software. Measures were performed in circular regions of interest delineating neuronal soma. For the calculation of $\Delta F/F$ over time, fluorescence intensity was measured in control zones of equal surfaces positioned beside each cell. The calcium imaging experiment was repeated on 8 males and 1 female (11 to 21-week-old, 3-4 week after surgery) during the blockade of the synaptic transmission with 1 μ M strychnine, 10 μ M DNQX, 50 μ M DL-AP5 and 50 μ M picrotoxin. Stock solutions of the pharmacological blockers were prepared as follow: 50 mM Picrotoxin in DMSO, 10 mM DNQX, 10 mM strychnine and 50 mM DL-AP5 in nanopure water.

Ex-vivo patch-clamp experiments

Fourteen males and six females (8 to 12-week-old) were used for patch-clamp experiments. Brain slices were prepared as described for the calcium imaging experiments. The same Olympus microscope equipped with specific filters allowing the visualization of Alexa-Fluor 488 and mCherry labeled neurons with the EMCCD camera was used for these experiments. Brain slices were superfused for 7 minutes with ACSF solutions containing 5, 3.5, 2 or 0.5 mM glucose maintained at 32-34 °C. The osmolarity of the solutions was compensated with sucrose (12.5, 14, 15.5 or 17 mM respectively). Borosilicate pipettes (resistance: 2-5 M Ω ; GC150F-7.5, Harvard Apparatus, Harvard Bioscience, Holliston, MA, USA) were prepared with a P-97 horizontal micropipette puller (Sutter Instrument, Novato, CA, USA). In current-clamp experiments, the holding current was set to zero and the patch pipettes were filled with an intrapipette containing (in mM): 130 K-gluconate, 5 NaCl, 1 $MgCl_2$, 10 NaPhosphocreatinine, 10 HEPES, 0.2 EGTA, 4 MgATP, 0.5 Na_2GTP (pH 7.2-7.4; 285 ± 5 mOsm). Series resistances were not compensated.

For the measurement of the optogenetically evoked EPSCs in voltage-clamp mode, ten $Gck^{cre/+}$ males (10-12 weeks-old) infused with an AAV2-*Ef1 α -DIO-ChR2(H134R)-eYFP-WPRE-pA* in the PVT 3-5 weeks before the experiments were used. After establishing the whole-cell configuration, medium spiny neurons of the NAc were clamped at -70mV and light-induced currents were recorded with an intrapipette solution

containing (in mM) 117 cesium methanesulfonate, 20 HEPES, 5 tetraethylammonium-Cl, 2.8 NaCl, 0.4 EGTA, 5 MgATP and 0.5 Na₂GTP (pH 7.2-7.4; 285 ± 5 mOsm). To activate neuronal terminals, brain slices were exposed to 4ms 473 nm blue light pulses delivered every 10s with the blue LED system described above. Data were acquired with a MultiClamp 700B amplifier and a Digidata 1440A analog/digital interface operated by pClamp 10 data acquisition software (Molecular Devices, San Jose, CA, USA) with a 10000 Hz sampling rate.

In vivo chemogenetics

The hM4Di DREADD experiment started 3 weeks after surgeries (described above) and was performed 2 h after the beginning of the scotophase (reverse light/dark cycle, light on at 7 a.m.) at a constant temperature (22 ± 1 °C) and relative humidity (49 ± 8%). For this experiment, we used 13-week-old males *Gck^{cre/+}* and *Gck^{+/+}* control littermates. Mice had *ad libitum* access to water and food (Diet 3436, Kliba Nafag) outside and during the test periods.

Animals were overnight fasted prior to the start of the experiment. Clozapine was administered via intraperitoneal (i.p.) injection (C6305, Sigma Aldrich, Saint Louis, USA, 0.1 mg/kg) 30 min prior to be placed in housing cage of the BioDAQ system (Research Diets, Inc). Food intake was monitored during 24 h and data were exported in 1-hour bins.

In vivo optogenetics

Experiments were essentially carried out as in Labouèbe et al. (Labouèbe et al., 2016). 10 to 12-week old males *Gck^{cre/+}* or *Gck^{+/+}* control littermates were used for *in vivo* optogenetics. Animals were isolated in housing cages to prevent any damage of the implanted cannula. Experiments started 3 weeks after surgeries (described above) and were performed 3-8 h after the beginning of the scotophase (reverse light/dark cycle, light on at 7 a. m.) with the same temperature (22 ± 1°C) and relative humidity (49 ± 8%) as for the chemogenetic experiment. Animals had *ad libitum* access to water and food outside the test periods. A DPSS laser (LRS-0473; Laserglow Technologies, Toronto, Canada) was used to deliver light pulses (10 ms light pulses at 20 Hz; 1s on/1 s off; 10–15 mW; 473 nm) through 2 patch cords (0.22 NA; 200 μm core diameter; Doric Lenses, Québec, Canada) connected to the optic fiber cannulas. When used, light stimulations were applied during the entire duration of the experimental session. To prevent the patch cords from twisting and to allow mice to move freely, a rotary joint (FRJ 1x2i_FC_2FC; Doric Lenses) was placed outside the operant conditioning chamber right on top of the animal. Injection sites and optical fiber cannula implantations were verified for each mouse at the end of the experiment.

Mice were trained in operant conditioning chambers (Med Associates, Fairfax, VA, USA). Animals had a choice between an active nosepoke hole associated with a 3 s light cue allowing the delivery of a 10 μl of a 10 % sucrose reward solution through a central spout equipped with an infrared head entry detector and an inactive nosepoke hole that remained inoperative. Liquid rewards remained available for 3 s once access to the central spout was detected. During the first 8 days of testing, animals were trained under a fixed ratio 1 schedule of reinforcement (FR1, 30 min daily sessions) in the absence of any light stimulation and with the patch cords not connected to the implanted optic fiber cannula. To enhance motivation for sucrose, animals were slightly food restricted (~2.8 g of normal chow per day, Diet 3436, Kliba Nafag) during this learning phase. After this, the number of rewards and number of active nosepokes performed by mice under an FR1 schedule (30 min daily sessions) were quantified during light stimulations. For this, animals were fed *ad libitum* with normal chow diet. Mice were tested during 7 consecutive days with 20 Hz light stimulations followed by 2 days at 40 Hz. Then, the animals underwent three consecutive sessions (90 min daily sessions) under a progressive-ratio schedule of reinforcement (PR) at 40 Hz. With this schedule, the number of active nosepokes to obtain a reward increases exponentially between rewards following the equation given by: (Labouèbe et al., 2016; Richardson and Roberts, 1996):

$$\text{Response ratio} = (5 \cdot e^{(\text{reward} \cdot 0.2)}) - 5$$

For the experiments performed under PR schedule, the number of daily rewards, active nosepokes and the maximal operant responses (breakpoint values) were averaged for each animal over the 3 consecutive days of testing.

QUANTIFICATION AND STATISTICAL ANALYSIS

Quantification of the calcium transients from the ex-vivo calcium imaging experiments

The calcium spikes were detected with Matlab (R2016a, The MathWorks, Inc., Natick, MA, USA). Considering a normal distribution of noise frequencies, the standard deviation of the background noise was estimated using:

$$\hat{\sigma} = 1.4826 \cdot \text{MAD}(R(t))$$

Each recording was then normalized using:

$$\widetilde{R}(t) = \frac{R(t)}{\hat{\sigma}}$$

where $R(t)$ is the $\Delta F/F$ over time and MAD the median absolute deviation. Calcium spikes were detected with peakfinder with visually adjusted thresholds from unfiltered normalized recordings. Quantification of the firing frequency was made during the last 5 minutes of the two time periods with the 2.5 mM glucose baseline condition. At 0.1 mM, spike frequency was quantified during a 5 minutes period around the peak of the response for GI neurons while the last 5 minutes were considered for GE and NR neurons respectively.

Current-clamp mode recordings analysis

For patch-clamp recordings performed in current-clamp mode, the membrane potential (V_m) and spike frequency were quantified for each 30 s sweep. V_m was defined as the median of the membrane potential, previously filtered with a moving median filter (0.4 s sliding window) to remove the spiking events. For the detection of the spikes, the recordings were first band-pass filtered at 1-3000 Hz with a second order butterworth filter designed with the butter function. Normalization of the recordings was performed as described for the calcium imaging signals. Action potentials were then detected using the peakfinder function with adequate thresholds adjusted for each 30 s sweep of recordings.

Neuronal responses to change in the glucose concentration were then investigated using R (v.3.5.1). For both GE and GI, V_m and spike frequency values included in a 2.5 min time window (5 data points) around the minimum or maximum V_m value respectively, were detected for each of the low glucose concentrations tested (i.e. 3.5, 2 and 0.5 mM). These values were then compared to the values recorded during the last 2.5 min of each of the 5 mM glucose baselines. A neuron was considered as a GE or a GI if a significant hyperpolarization/depolarization of the membrane potential was observed between 5 mM and 0.5 mM glucose. Significance was assessed with a Welch's unpaired T-test. To be considered as a GE or a GI, the neurons should recover, at least partially, their initial V_m when glucose was switched back to the 5 mM glucose baseline (visual observations). Recordings from neurons that failed to recover their initial membrane potential at the end of the experiment were excluded from the data set.

Ex-vivo recordings in voltage-clamp mode

Light-evoked EPSC amplitude was calculated as the difference between the I_m value at the minima of each evoked EPSC and the median I_m during a 1s window preceding each EPSC. For each neuron, data were averaged over 15 EPSCs recorded during the last 2.5 min of each treatment.

Statistical analysis

All statistical analyses and graphical representations of data were performed with R software (v 3.5.1) (R Core Team, 2018). Data from current-clamp recordings, calcium imaging and behavioral experiments were analyzed with Linear Mixed Models using Penalized Quasi-Likelihood with the glmmPQL function from the MASS package (Venables and Ripley, 2002). Poisson family with log link were used for count data while the other sets of data were analyzed with Gaussian Family and identity link. To compare the proportion of GE and GI in the calcium imaging experiments in the presence vs. absence of the synaptic inhibitors (binary data), GLMs with binomial family and logit link were used. Data with evoked EPSCs measured with voltage-clamp recordings were analyzed with linear mixed-effect models with the lme function from the nlme package (Pinheiro et al., 2018). As most of our data comprised measurements from many time points from each animal or neurons, mixed effects modeling was used to account for the non-independence of the data. Glucose concentrations, time points and/or genotype and their interactions were

treated as fixed factors while mouse or neurons were included as random effects. Appropriate distribution of the standardized residuals over the fitted values were checked for all models. When multicomparisons were made, p values were adjusted with the Benjamini-Hochberg method. Data are shown as mean \pm standard error of the mean (SEM) or box plots representing the lower quartile (Q1), median (Q2), upper quartile (Q3) and lowest and highest data points still within 1.5 of the interquartile range (whiskers). All graphical representations were made with the ggplot2 package ([Wickham, 2016](#)).